nature ecology & evolution

ARTICLES

https://doi.org/10.1038/s41559-018-0518-2

Homo sapiens in Arabia by 85,000 years ago

Huw S. Groucutt[1,2*], Rainer Grün[3,4], Iyad S. A. Zalmout[5], Nick A. Drake[2,6], Simon J. Armitage[7,8], Ian Candy[7], Richard Clark-Wilson[7], Julien Louys[3], Paul S. Breeze[6], Mathieu Duval[3,9], Laura T. Buck[10,11], Tracy L. Kivell[12,13], Emma Pomeroy[10,14], Nicholas B. Stephens[13], Jay T. Stock[10,15], Mathew Stewart[16], Gilbert J. Price[17], Leslie Kinsley[4], Wing Wai Sung[18], Abdullah Alsharekh[19], Abdulaziz Al-Omari[20], Muhammad Zahir[21], Abdullah M. Memesh[5], Ammar J. Abdulshakoor[5], Abdu M. Al-Masari[5], Ahmed A. Bahameem[5], Khaled S. M. Al Murayyi[20], Badr Zahrani[20], Eleanor M. L. Scerri[1,2] and Michael D. Petraglia[2,22*]

Understanding the timing and character of the expansion of *Homo sapiens* out of Africa is critical for inferring the colonization and admixture processes that underpin global population history. It has been argued that dispersal out of Africa had an early phase, particularly ~130–90 thousand years ago (ka), that reached only the East Mediterranean Levant, and a later phase, ~60–50 ka, that extended across the diverse environments of Eurasia to Sahul. However, recent findings from East Asia and Sahul challenge this model. Here we show that *H. sapiens* was in the Arabian Peninsula before 85 ka. We describe the Al Wusta-1 (AW-1) intermediate phalanx from the site of Al Wusta in the Nefud desert, Saudi Arabia. AW-1 is the oldest directly dated fossil of our species outside Africa and the Levant. The palaeoenvironmental context of Al Wusta demonstrates that *H. sapiens* using Middle Palaeolithic stone tools dispersed into Arabia during a phase of increased precipitation driven by orbital forcing, in association with a primarily African fauna. A Bayesian model incorporating independent chronometric age estimates indicates a chronology for Al Wusta of ~95–86 ka, which we correlate with a humid episode in the later part of Marine Isotope Stage 5 known from various regional records. Al Wusta shows that early dispersals were more spatially and temporally extensive than previously thought. Early *H. sapiens* dispersals out of Africa were not limited to winter rainfall-fed Levantine Mediterranean woodlands immediately adjacent to Africa, but extended deep into the semi-arid grasslands of Arabia, facilitated by periods of enhanced monsoonal rainfall.

Homo sapiens evolved in Africa in the late Middle Pleistocene[1]. Early dispersals out of Africa are evidenced at the Levantine site of Misliya at ~194–177 thousand years ago (ka)[2], followed by Skhul and Qafzeh, where *H. sapiens* fossils have been dated to ~130–100 and ~100–90 ka, respectively[3]. Although the fossil evidence from the Levant has been viewed as the onset of a much broader dispersal into Asia[4–6], it has generally been seen as representing short-lived incursions into the woodlands of the Levant immediately adjacent to Africa, where relatively high precipitation is produced by winter storms tracking across the Mediterranean[7,8]. While the Levantine record indicates the subsequent local replacement of early *H. sapiens* by Neanderthals, the failure of early dispersals to extend beyond the Levant is largely inferred from interpretations of genetic data[9]. Genetic studies have suggested that recent non-African populations stem largely[10], if not entirely[9], from an expansion ~60–50 ka, but this model remains debated. The absence of low-latitude Pleistocene human DNA and uncertainties regarding ancient population structure undermine conclusions drawn from genetic studies alone. The paucity of securely dated archaeological, palaeontological and ancient DNA data—particularly across southern Asia—has made testing dispersal hypotheses challenging[4,7,11].

Recent fossil discoveries in East Asia indicate that the early (particularly Marine Isotope Stage 5, MIS5) dispersals of *H. sapiens* extended across much of southern Asia. At Tam Pa Ling in Laos, *H. sapiens* fossils date to between 70 and 46 ka[12]. Teeth assigned to *H. sapiens* from Lida Ajer cave, Sumatra, were recovered from a breccia dating to 68 ± 5 ka, with fauna from the site dating to

[1]School of Archaeology, Research Laboratory for Archaeology and the History of Art, University of Oxford, Oxford, UK. [2]Department of Archaeology, Max Planck Institute for the Science of Human History, Jena, Germany. [3]Australian Research Centre for Human Evolution (ARCHE), Environmental Futures Research Institute, Griffith University, Nathan, Queensland, Australia. [4]Research School of Earth Sciences, The Australian National University, Canberra, Australian Capital Territory, Australia. [5]Saudi Geological Survey, Sedimentary Rocks and Palaeontology Department, Jeddah, Saudi Arabia. [6]Department of Geography, King's College London, London, UK. [7]Department of Geography, Royal Holloway, University of London, London, UK. [8]SFF Centre for Early Sapiens Behaviour (SapienCE), University of Bergen, Bergen, Norway. [9]Geochronology, Centro Nacional de Investigación sobre la Evolución (CENIEH), Burgos, Spain. [10]PAVE Research Group, Department of Archaeology, University of Cambridge, Cambridge, UK. [11]Earth Sciences Department, Natural History Museum, London, UK. [12]Skeletal Biology Research Centre, School of Anthropology and Conservation, University of Kent, Canterbury, UK. [13]Department of Human Evolution, Max Planck Institute for Evolutionary Anthropology, Leipzig, Germany. [14]School of Natural Sciences and Psychology, Liverpool John Moores University, Liverpool, UK. [15]Department of Anthropology, University of Western Ontario, London, Ontario, Canada. [16]Palaeontology, Geobiology and Earth Archives Research Centre, School of Biological, Earth and Environmental Science, University of New South Wales, Sydney, New South Wales, Australia. [17]School of Earth and Environmental Sciences, The University of Queensland, St Lucia, Queensland, Australia. [18]Department of Life Sciences, Natural History Museum, London, UK. [19]Department of Archaeology, King Saud University, Riyadh, Saudi Arabia. [20]Saudi Commission for Tourism and National Heritage, Riyadh, Saudi Arabia. [21]Department of Archaeology, Hazara University, Mansehra, Pakistan. [22]Human Origins Program, National Museum of Natural History, Smithsonian Institution, Washington DC, USA. *e-mail: huw.groucutt@rlaha.ox.ac.uk; petraglia@shh.mpg.de

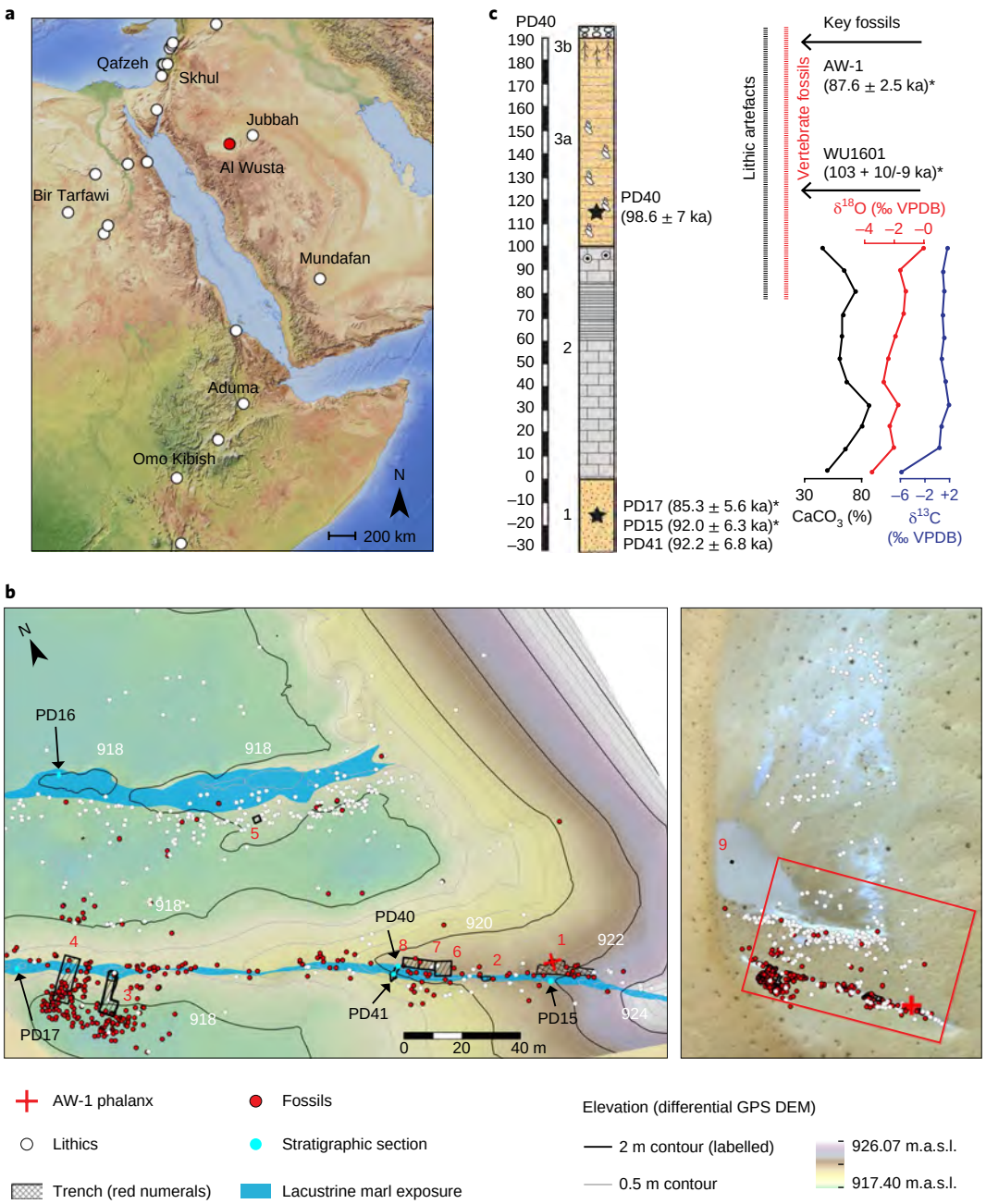

Fig. 1 | Al Wusta location, map of site and stratigraphy. a, The location of Al Wusta and other key MIS5 sites in the region[11]. **b**, Al Wusta digital elevation model (DEM) showing the location of the AW-1 phalanx, marl beds, lithics and vertebrate fossils, and the locations of the trenches and sections. The inset shows a satellite image of the whole site. Sources: Esri, DigitalGlobe, GeoEye, i-cubed, USDA FSA, USGS, AEX, Getmapping, Aerogrid, IGN, IGP, swisstopo and the GIS User Community. **c**, A stratigraphic log of Al Wusta showing the sedimentology of the exposed carbonate beds, isotopic values, OSL ages for sand beds and U-series and ESR ages for AW-1 and WU-1601. Sands are shown in yellow: lower massive sands are aeolian (Unit 1), and upper laminated sands are water-lain (Unit 3a) and have been locally winnowed to generate a coarse desert pavement (Unit 3b); lacustrine marls are shown (Unit 2) in grey (for the full key and description, see Supplementary Figs. 13 and 14 and Supplementary Information 5). Section PD40 is shown as it contains the thickest sequence and is most representative of Al Wusta; chronometric age estimates (marked with an asterisk) from the site are depicted in their relative stratigraphic position (see Supplementary Fig. 14 for their absolute positions).

75 ± 5 ka (ref. [13]). Several sites in China have produced fossil material claimed to represent early *H. sapiens*[14]. Examples include teeth from Fuyan Cave argued to be older than 80 ka on the basis of the dating of an overlying speleothem a few metres from the fossils[15], and teeth from Luna Cave that were found in a layer dating to between 129.9 ± 1.5 ka and 70.2 ± 1.4 ka (ref. [16]). Teeth and a mandible from Zhiren Cave, China, date to at least 100 ka and have been argued to represent *H. sapiens*, but other species attributions are possible[17].

The recent documentation of a human presence in Australia from ~65 ka is consistent with these findings[18]. Likewise, some interpretations of genetic data are consistent with an early spread of *H. sapiens* across southern Asia[10]. These discoveries are leading to a radical revision of our understanding of the dispersal of *H. sapiens*, yet there remain stratigraphic and taxonomic uncertainties for many of the East Asian fossils[14,19], and thousands of kilometres separate these findings from Africa.

The Arabian Peninsula is a vast landmass at the crossroads of Africa and Eurasia. Growing archaeological evidence demonstrates repeated hominin occupations of Arabia[20,21] each associated with a strengthened summer monsoon that led to the reactivation of lakes and rivers[22–24], as it did in North Africa[25]. Here we report the discovery of the first pre-Holocene human fossil in Arabia, Al Wusta-1 (AW-1), as well as the age, stratigraphy, vertebrate fossils and stone tools at the Al Wusta site (Fig. 1, see also Supplementary Information).

Results

AW-1 is an intermediate manual phalanx, most likely from the third ray (Fig. 2a and Supplementary Information 1; see below for detail on siding and species identification). It is generally well preserved, although there is some erosion of the cortical/subchondral bone, and minor pathological bone formation (probably an enthesophyte) affecting part of the diaphysis (Supplementary Information 1). The phalanx measures 32.3 mm in proximo-distal length, and 8.7 mm and 8.5 mm in radio-ulnar breadth of the proximal base and mid-shaft, respectively (Supplementary Table 1).

AW-1 is more gracile than the robust intermediate phalanges of Neanderthals[26–28], which are broader radio-ulnarly relative to their length and have a more 'flared' base. AW-1's proximal radio-ulnar maximum breadth is 14.98 mm, which provides an intermediate phalanx breadth–length index (proximal radio-ulnar maximum breadth relative to articular length) of 49.6. This is very similar to the mean (±s.d.) for the Skhul and Qafzeh *H. sapiens* of 49.7 (±4.1) and 49.1 (±4.0) for Upper Palaeolithic Europeans, but 1.89 standard deviations below the Neanderthal mean of 58.3 (±4.6)[29].

To provide a broad interpretive context for the Al Wusta phalanx, we conducted linear and geometric morphometric (GMM) landmark analyses (Supplementary Information 1) on phalanges from non-human primates, fossil hominins and geographically widespread recent *H. sapiens*. Comparative linear analyses (Supplementary Information 1, Supplementary Tables 2 and 3 and Supplementary Fig. 1) reveal that there is substantial overlap across most taxa for all shape ratios, so AW-1 falls within the range of variation of *H. sapiens*, cercopiths, *Gorilla*, *Australipithecus afarensis*, *Australipithecus sediba* and Neanderthals. However, AW-1 is most similar to the median value or falls within the range of variation of recent and early *H. sapiens* for all shape ratios.

GMM analyses of AW-1 and various primate groups including hominins (see Supplementary Table 4 and Supplementary Fig. 2 for landmarks, and Supplementary Table 5 for sample) are illustrated in Fig. 3 and Supplementary Fig. 3. Principal component 1 (PC1) and PC2 together account for 61% of group variance in shape. AW-1 is separated on these two shape vectors from the non-human primates and most of the Neanderthals. AW-1 falls closest to the recent and early *H. sapiens* and is clearly differentiated from all non-human primates. This is also shown by the Procrustes distances from AW-1 to the mean shapes of each taxonomic group (Supplementary Table 6).

Three of the Neanderthal phalanges (from Kebara 2 and Tabun C1) are quite disparate from the main Neanderthal cluster and fall closer to the *H. sapiens* and Al Wusta cluster on PC1 and PC2 (Fig. 3 and Supplementary Fig. 3). Having established the hominin affinity of AW-1, shape was analysed in more detail using a smaller hominin sample for which ray number and side were known, which included Kebara 2 and Tabun C1. The broader primate sample used in the first GMM analysis was not used for the more detailed shape analysis, as the initial comparisons show clearly that AW-1 is not a non-human primate and including this level of variation could potentially mask more subtle shape differences between hominins. The side and ray are also not known for most of the Neanderthal and non-human primate samples, meaning it would be impossible to evaluate the effect of these factors using this sample.

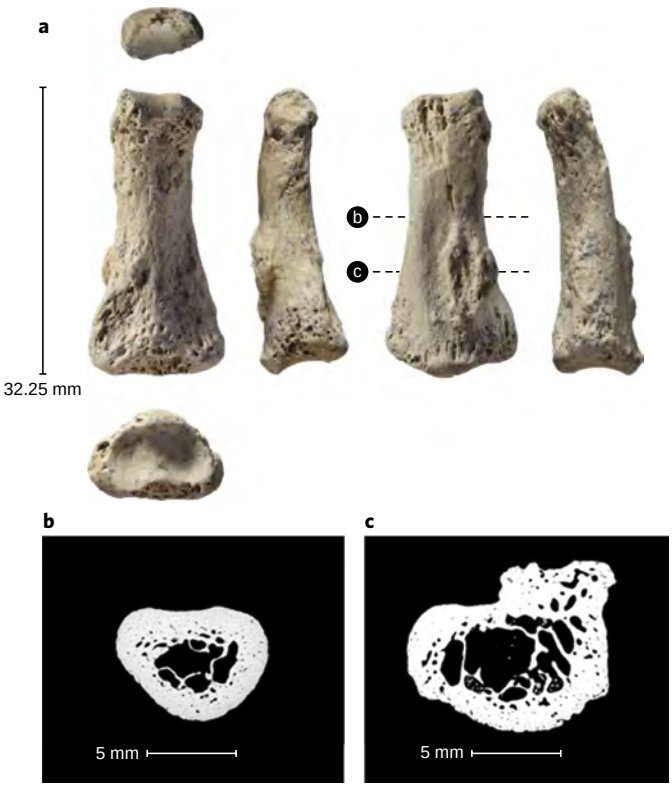

Fig. 2 | Photographs and micro-computed tomography scans of the AW-1 *H. sapiens* phalanx. a, Photographs in (left column, top to bottom) distal, palmar and proximal views, and (middle row, left to right) lateral 1, dorsal and lateral 2 views. **b**,**c**, Micro-computed tomography cross-sections (illustrated at ×2 magnification) 54% from the proximal end (**b**) and illustrating abnormal bone (**c**).

The more in-depth shape comparison and modelling using the hominin sample of phalanges of known ray and side (Supplementary Table 7) demonstrates that the long and slender morphology of AW-1 falls just outside the range of variation of comparative Middle Palaeolithic modern humans, but that its affinity is clearly with *H. sapiens* rather than Neanderthals (Fig. 4 and Supplementary Table 8). Although both Pleistocene *H. sapiens* and Neanderthal landmark configurations fall almost completely inside the scatter for the Holocene *H. sapiens* sample in the principal components analysis (Fig. 4), AW-1 is closest to Holocene *H. sapiens* third intermediate phalanges. AW-1 overlaps with the Holocene *H. sapiens* sample, but is separated from the Pleistocene *H. sapiens* specimens by a higher score on PC2 and from the Neanderthal group by a simultaneously higher score on PC1 and PC2. The Procrustes distances (Supplementary Table 8) also show that AW-1 is most distinct from the Neanderthal phalanges, which fall towards the lower ends of both principal components and are characterized by shorter and broader dimensions. PC1 and PC2 in this analysis show that AW-1 is taller and narrower (in all directions: dorso-palmarly, proximo-distally and radio-ulnarly) than almost all of the phalanges in the comparative sample and is particularly distinct from most of the Neanderthal phalanges. In this analysis, AW-1 is closest in shape to the third phalanges of individuals from (in descending order of proximity) Egyptian Nubia, and Medieval Canterbury (UK) and Maiden Castle (Iron Age Dorset, UK) (Supplementary Table 9), although there is not a great difference in its distance to any of these specimens. These analyses suggest that the AW-1 phalanx is likely to be a third intermediate phalanx from a *H. sapiens* individual.

The third ray is the most symmetrical ray in the hand and is therefore difficult to side, particularly when not all of the phalanges of a particular individual are present. Comparing AW-1 separately

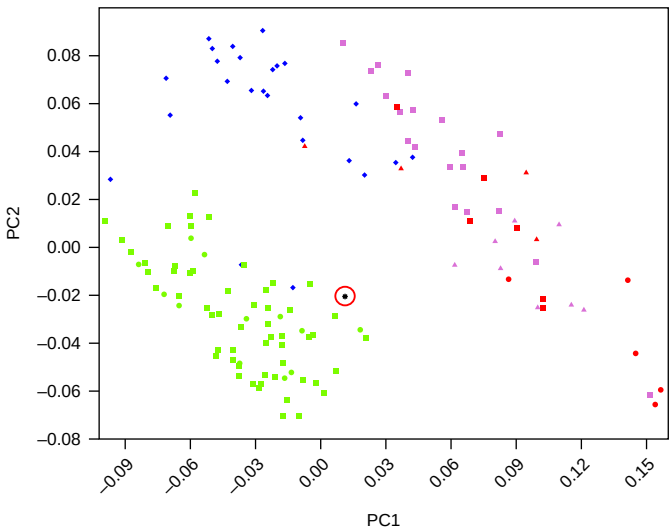

Fig. 3 | Scatterplot of the first two principal component scores of the geometric morphometric analysis of the AW-1 phalanx compared with a sample of primates, including hominins. Non-human hominoids: lilac; *Gorilla*: circles, *Pan*: triangles. Cercopithecoids: red; *Colobus*: triangles, *Mandrillus*: squares, *Papio*: circles. Neanderthals: blue diamonds. *H. sapiens*: green; early *H. sapiens*: circles, Holocene *H. sapiens*: squares. AW-1: black star, circled in red.

to right and to left phalanges (Supplementary Information 1.4) gives results that are very similar to the pooled sample, such that AW-1 is closest to Holocene *H. sapiens* third rays for both right and left hands (Supplementary Fig. 4 and Supplementary Table 10). There is little difference in morphological closeness between AW-1 and its nearest neighbour in the samples of right and left bones (Supplementary Table 11), reflecting the lack of difference in morphology between the sides. It is therefore not possible to suggest whether AW-1 comes from a right or a left hand using these analyses.

AW-1 is unusual in its more circular midshaft cross-sectional shape (Fig. 2b), which is confirmed by cross-sectional geometric analyses (Supplementary Information 1.5). This may reflect the pronounced palmar median bar that makes the palmar surface slightly convex at the midshaft rather than flat, the latter being typical of most later *Homo* intermediate phalanges. However, more circular shafts may reflect greater loading of the bone in multiple directions and enthesophytes are a common response to stress from high levels of physical activity[30]. This morphology may reflect high and varied loading of the fingers during intense manual activity.

To determine the age of AW-1, and associated sediments and fossils, we used a combination of uranium series (U-series), electron spin resonance (ESR) and optically stimulated luminescence (OSL) dating (Methods and Supplementary Information 2 and 3). U-series ages were produced for AW-1 itself (87.6 ± 2.5 ka) and hippopotamus dental tissues (WU1601), which yielded ages of 83.5 ± 8.1 ka (enamel) and 65.0 ± 2.1 ka (dentine). They should be regarded as minimum estimates for the age of the fossils. In addition, a combined U-series–ESR age calculation for WU1601 yielded an age of 103 +10/−9 ka. AW-1 was found on an exposure of Unit 3b, and WU1601 was excavated from Unit 3a, 1 m away (Fig. 1b). Unit 1 yielded OSL ages of 85.3 ± 5.6 ka (PD17), 92.2 ± 6.8 ka (PD41) and 92.0 ± 6.3 ka (PD15), while Unit 3a yielded an OSL age of 98.6 ± 7.0 ka (PD40). The OSL age estimates agree within error with the U-series–ESR age obtained for WU-1601 and the minimum age of ~88 ka obtained for AW-1. These data were incorporated into a Bayesian sequential phase model[31] that indicates that deposition of Unit 1 ceased 93.1 ± 2.6 ka (Phase 1: PD15, 17, 41) and that Units 2 and 3 and all associated fossils were deposited between 92.2 ± 2.6 ka and 90.4 ± 3.9 ka (Phase 2: all other ages) (Supplementary Information 4 and Supplementary Fig. 11).

This ~95–86 ka timeframe is slightly earlier than most other records of increased humidity in the region in late MIS5[32,33], which correlate with a strengthened summer monsoon associated with an insolation peak at 84 ka. The underlying (Unit 1) aeolian sand layer at Al Wusta correlates with an insolation minimum at the end of MIS5c. The chronometric age estimates for the site suggest that lake formation and the

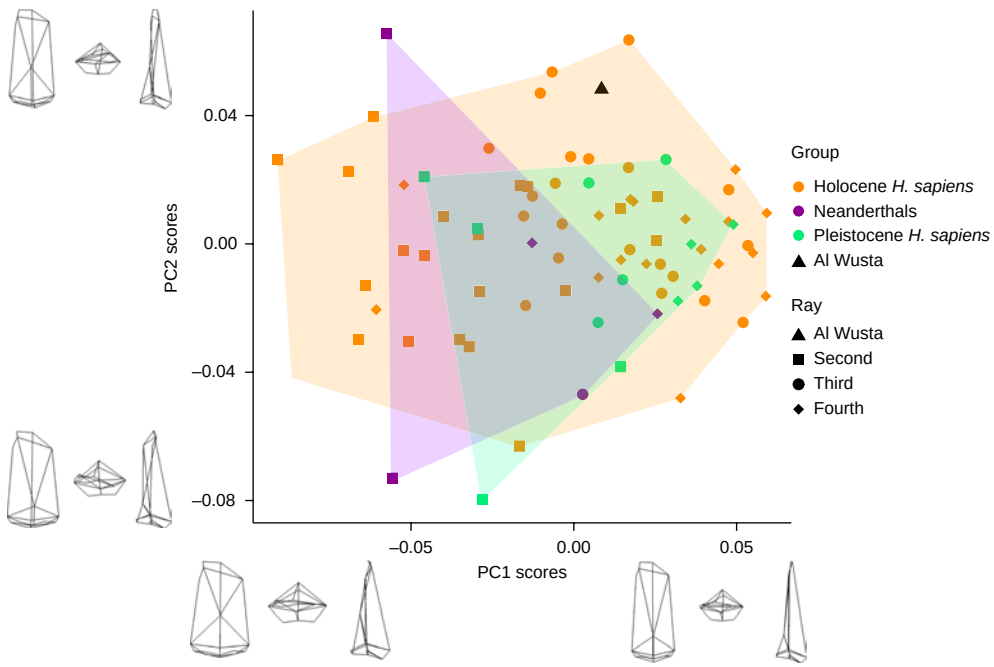

Fig. 4 | Scatterplot of the first two principal component scores from the geometric morphometric analyses of AW-1 and a sample of comparative hominin second, third and fourth intermediate phalanges. The wireframes show the mean configuration warped to the extremes of the principal component axes in dorsal (left), proximal (middle) and lateral (right) views. Convex hulls were added post hoc to aid visualization.

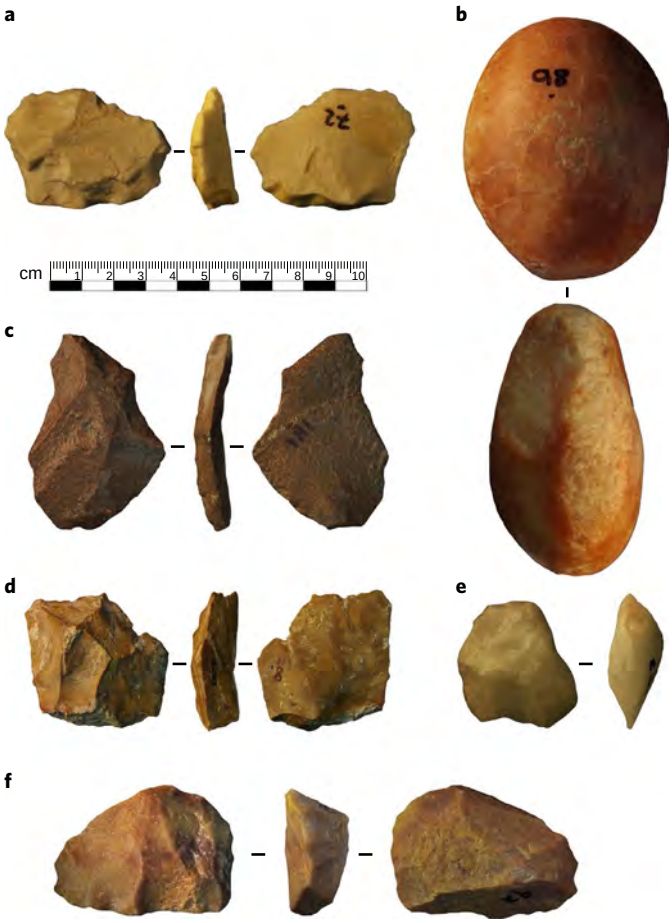

Fig. 5 | Selected Al Wusta lithic artefacts. a, Argillaceous quartzite flake. **b**, Quartz hammerstone. **c**, Ferruginous quartzite Levallois flake. **d**, Chert Levallois flake. **e**, Quartz recurrent centripetal Levallois core. **f**, Quartzite preferential Levallois core with centripetal preparation and pointed preferential removal.

associated fauna and human occupation occurred shortly after this in time. Regional indications of increased humidity around the 84 ka insolation peak include speleothem formation at ~88 ka in the Negev[34], and the formation of sapropel S3 beginning ~86 ka (ref. [35]). In both the Levant and Arabia, records are consistent with this switch from aridity to humidity around this time[32–40]. Precisely reconstructing regional palaeoclimate at this time and relating it to human demographic and behavioural change has proved challenging. This reflects both rapid changes in climate, and the complexities involved in dating relevant deposits[41]. In summary, combining chronological data (Supplementary Sections 2–4), interpretation of the sedimentary sequence (described below) and the regional setting of Al Wusta, we conclude that lake formation and associated finds such as the AW-1 phalanx relate to the late MIS5 humid period associated with the 84 ka insolation peak.

The sedimentary sequence at Al Wusta consists of a basin-like deposit of exposed carbonate-rich sediments (Unit 2, 0.4–0.8 m thick), underlain by wind-blown sand (Unit 1) and overlain by water-lain sands (Unit 3). The carbonate-rich sediments of Unit 2 are interpreted as lacustrine marl deposits on the basis of their sedimentology, geochemistry and diatom palaeoecology (Fig. 1c, Methods and Supplementary Information 5). At both the macro- and micro-scale, these beds are relatively massive and comprise fine-grained calcite, typical of material precipitating and accumulating in a still-water lacustrine environment[42]. At the micro-scale there is no evidence for the desiccation or fluctuation of water levels typical of palustrine/wetland environments[42], implying that the lake body was perennial. The diatom flora support this, containing species such as *Aulacoseira italica* and *Aulacoseira granulata* throughout the sequences, indicating an alkaline lake a few metres deep. The water was fresh, not saline or brackish, since saline-tolerant species and evaporitic minerals are absent throughout. While the oxygen and carbon isotopic values ($\delta^{18}O$ and $\delta^{13}C$) of continental carbonates are controlled by a wide range of variables, the values derived from the Al Wusta marl beds are compatible with the suggestion of marls precipitated in a perennial lake basin. The Al Wusta carbonate beds therefore indicate a perennial lake body a few metres in depth. The existence of a marl-precipitating lake basin implies that this system was groundwater fed (to allow for sufficient dissolved mineral material to be present in the lake waters). Although the Al Wusta sequence represents a single lake basin, the development of such a feature over highly permeable aeolian sands in a region where no lake systems exist at the present day implies a local increase in the water table that would require an increase in mean annual rainfall. Consequently, the Al Wusta sequence represents the occurrence of a humid interval at this time. The Unit 2 marl is overlain by a medium-coarse sand (Unit 3) with crude horizontal laminations, occasional clasts, fragments of ripped up marl and shells of *Melanoides tuberculata* and *Planorbis* sp. While some vertebrate fossils and lithics were found in the upper part of Unit 2, most were found in or on the surface of Unit 3. Unit 3a sands are water-lain and represent the encroachment of fluvial sediment as the lake environment shallowed and contracted. Unit 3b represents a winnowed lag formed by aeolian deflation of 3a. The sequence is capped by a dense network of calcitic rhizoliths marking the onset of fully terrestrial conditions.

A total of 860 vertebrate fossils were excavated from Unit 3 and the top of Unit 2 ($n = 371$) and systematically surface-collected ($n = 489$). These include specimens attributed to Reptilia, Aves and Mammalia (Supplementary Table 19, Methods and Supplementary Information 6). Notable taxa now extinct in Arabia are predominately grazers and include *Hippopotamus*, *Pelorovis* and *Kobus*. The faunal community demonstrates a clear preference for temperate to semi-arid grasslands, and the presence of *Hippopotamus* and *Kobus* indicates permanent muddy, fluvial or lacustrine conditions[43] not currently found in the Nefud desert, but consistent with the geological evidence from the site. The faunal assemblages show a strong affinity to African fauna, particularly *Hippopotamus, Pelorovis* and *Kobus*[44]. Many large tooth pits on fossils indicate that large carnivores played a role in the accumulation of the deposit. Long bone circumference, completeness and the number of green fractures suggests modification of bones by bone-breaking agents such as large carnivores or hominins (Supplementary Information 6). However, no evidence of cut marks or hammerstone damage to the bones was observed.

An assemblage of 380 lithic artefacts (stone tools) was recovered from the excavation of upper Unit 2 and Unit 3 and systematic surface collection (Methods, Fig. 5 and Supplementary Information 7). They are of Middle Palaeolithic character and most are chert and quartzite. The assemblage demonstrates a focus on centripetal Levallois reduction, and is similar to other late MIS5 assemblages in the west and north of Arabia[45], and contemporaneous assemblages in east (for example, Aduma and BNS at Omo Kibish) and northeast Africa (for example, Bir Tarfawi), as well as those from the Levant (for example, Qafzeh)[11] (Fig. 5).

Discussion

AW-1 is the oldest directly dated *H. sapiens* fossil outside Africa and the Levant. It joins a small but growing corpus of evidence that the early dispersal of *H. sapiens* into Eurasia was much more widespread than previously thought. The site of Al Wusta is located in the Nefud desert more than 650 km southeast of Skhul and Qafzeh (Fig. 1a). This site establishes that *H. sapiens* were in Arabia in late MIS5, rather than being restricted to Africa and the Levant as suggested

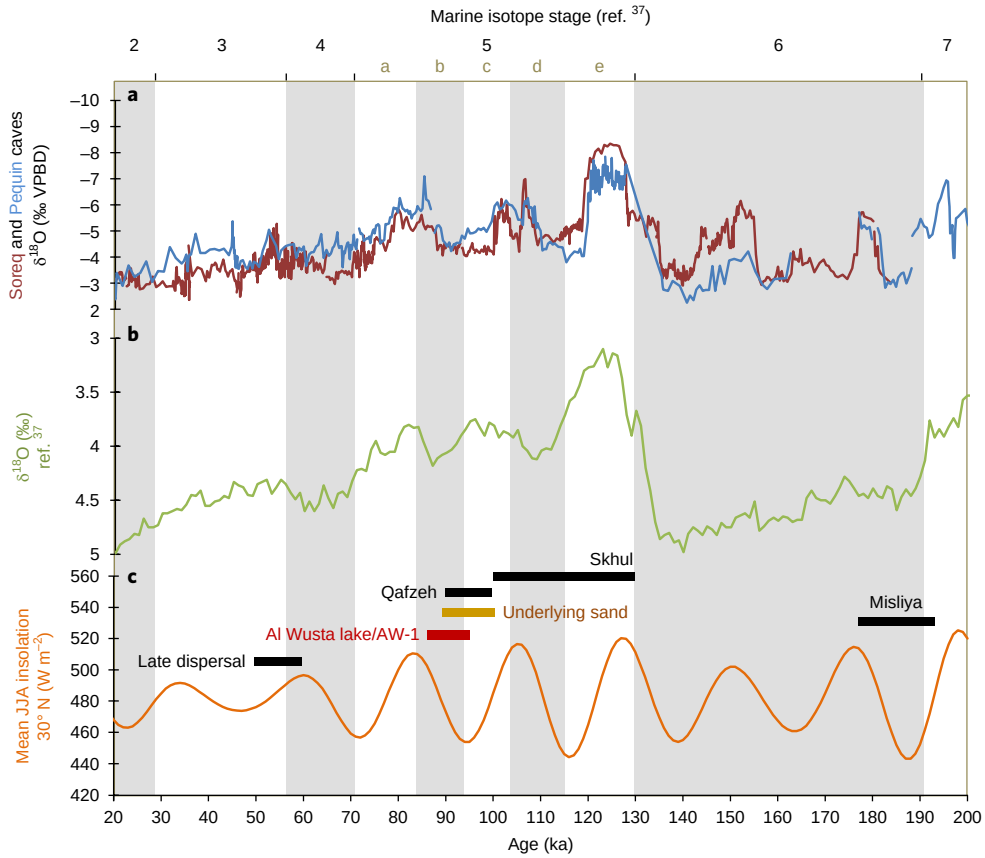

Fig. 6 | The chronological and climatic context of Al Wusta. The Al Wusta lake phase falls chronologically at the end of the time range of MIS5 sites from the Mediterranean woodland of the Levant (~130–90 ka) and earlier than the late dispersal(s) (~60–50 ka) as posited in particular by genetic studies. The chronology of these dispersals and occupations corresponds with periods of orbitally modulated humid phases in the eastern Mediterranean[36] that are important intervals for human dispersals into Eurasia, and are also proposed to correspond with episodes of monsoon-driven humidity in the Negev and Arabian desert[34]. Therefore, environmental amelioration of the Saharo-Arabian belt appears to be crucial for allowing occupation at key sites that document dispersal out of Africa. **a**, East Mediterranean speleothem $\delta^{18}O$ record from Soreq and Pequin caves[36]. **b**, Global $\delta^{18}O$ record[37]. **c**, Insolation at 30° N[38], showing the temporal position of key sites relating to dispersal out of Africa[2,3,11,48]. The chronology for Al Wusta shows the phases defined by the Bayesian model at 2σ. JJA, June–July–August.

by traditional models (Fig. 6). With Skhul dating to ~130–100 ka, Qafzeh to ~100–90 ka[3,46] and Al Wusta to ~95–85 ka, it is currently unclear whether the southwest Asian record reflects multiple early dispersals out of Africa or a long occupation during MIS5. The association of the Al Wusta site with a late MIS5 humid phase (Fig. 6) suggests that significant aspects of this dispersal process were facilitated by enhanced monsoonal rainfall. While changes in behaviour and demography are crucial to understanding the dispersal process, climatic windows of opportunity were also key in allowing *H. sapiens* to cross the Saharo-Arabian arid belt, which often constituted a formidable barrier[24,25].

Conclusion

Al Wusta shows that the early, MIS5, dispersals of *H. sapiens* out of Africa were not limited to the Levantine woodlands sustained by winter rainfall, but extended deep into the Arabian interior where enhanced summer rainfall created semi-arid grasslands containing abundant fauna and perennial lakes. After long being isolated in Africa[1,47,48], our species expanded into the diverse ecologies of Eurasia in the Late Pleistocene. Within a few thousand years of spreading into Eurasia, our species was occupying rainforest environments and making long sea crossings to remote islands[13,18]. Adapting to the semi-arid conditions of the Saharo-Arabian arid belt represented a crucial step on this pathway to global success and the Al Wusta *H. sapiens* fossil demonstrates this early ability to occupy diverse ecologies that led to us becoming a cosmopolitan species.

Methods

Site identification, survey and excavation. The site of Al Wusta (fi ld code WNEF16_30) was discovered in 2014 as part of a programme of joint fi ldwork of the Palaeodeserts Project, the Saudi Commission for Tourism and National Heritage, and the Saudi Geological Survey. It is located in the western Nefud desert, a few kilometres from the Middle Pleistocene fossil locality of Ti's al Ghaddah[49]. The locations of all materials of interest (fossils, stone tools, geomorphological features, excavations and sample points) were recorded using a high-precision Trimble XRS Pro Differential Global Positioning System and a total station, and entered into a geographic information system (Fig. 1). Elevation data (metres above sea level, m.a.s.l.) were recorded as a series of transects across the site, a digital elevation model produced, and contours interpolated (spline) from all data with precisions of better than 10 cm in all (x,y,z) dimensions (22,047 points). Th s allowed visualization and recording of the spatial relationships between materials in three dimensions (Fig. 1). Eight trenches were excavated into the fossil- and artefact-bearing deposits. These trenches revealed vertebrate remains and lithics, but no further human fossils were recovered.

Morphological analysis of the Al Wusta-1 phalanx. The phalanx was scanned using micro-computed tomography (micro-CT) on the Nikon Metrology XT H 225 ST High Resolution scanner and X-Tek software (Nikon Metrology) housed in the Cambridge Biotomography Centre, University of Cambridge, UK. Scan parameters were: a tungsten target; 0.5 mm copper filter; 150 kV; 210 mA; 1,080 projections with 1,000 ms exposure, and resulted in a voxel size of 0.02 mm^3. The micro-CT data were reconstructed using CT-PRO 3D software (Nikon Metrology) and exported as an image (.tif) stack. Other CT data were obtained from the

institutions cited in Supplementary Table 5 with permissions following the memoranda of understanding with each institution.

Three-dimensional landmarks and semilandmarks were chosen to best describe the overall shape of the morphology of the AW-1 phalanx (Supplementary Table 4 and Supplementary Fig. 2), and were digitized on virtual reconstructions of phalanges created from micro-CT data in AVIZO 8 and 9.1 (FEI Software). Landmark coordinates were exported for use in Morphologika[50]. In Morphologika, generalized Procrustes analyses were performed to superimpose landmark coordinate data, and principal components analyses were run to investigate similarities in shape between specimens. Shape differences along principal components were visualized and wireframes were produced in Morphologika; principal component scores were exported to create graphs in R[51]. Procrustes distances between specimens were calculated using MorphoJ[52]. To avoid representing the same phalanges from different sides of a single individual as independent data points and to maximize sample sizes in pooled analyses, right phalanges were used in cases where the phalanges from both sides were present. Where only the left was present, this was used and 'reflected' (that is, mirrored) in Morphologika to generate landmark configurations consistent with right phalanges.

U-series and combined U-series–ESR dating of fossil bone and teeth. The AW-1 phalanx (laboratory number 3675) and a hippopotamus tooth fragment (laboratory number WU1601) were collected from Trench 1 (Fig. 1) for U-series and combined U-Series–ESR dating, respectively. The external dose rate utilized the data of OSL sample PD40, which was collected in an equivalent position within Unit 3a.

U-series analysis. U-series analyses were conducted at the Research School of Earth Sciences, The Australian National University, Canberra. The experimental set-up for the U-series analysis of the phalanx was described in detail previously[53] (Supplementary Figs. 2 and 3 and Supplementary Information 2). Laser ablation was used to drill a number of holes into AW-1 following the approach of an earlier study[54]. After a cleaning run with the laser set at a diameter of 460 µm, 7 holes were drilled for 1,000 s with the laser set at 330 µm. The isotopic data streams were converted into $^{230}Th/^{234}U$ and $^{234}U/^{238}U$ activity ratios and apparent Th/U age estimates and subsequently binned into 30 successive sections (each containing 33 cycles) for the calculation of average isotopic ratios and ages. A similar experimental set-up and methodology were employed for the laser ablation U-series analysis of tooth sample WU1601. The whole closed system U-series analytical data sets of the enamel and dentine sections were integrated to provide the data input for the ESR age calculations.

ESR dose evaluation. The ESR dose evaluation of the hippopotamus tooth was carried out at CENIEH, Burgos, Spain, following a similar procedure to that described previously[49]. Enamel was collected from WU1601 and powdered <200 µm. The sample was then divided into 11 aliquots and gamma-irradiated with a Gammacell-1000 Cs-137 source to increasing doses until 3.4 kGy. ESR measurements were carried out at room temperature with an EMXmicro 6/1 Bruker ESR spectrometer coupled to a standard rectangular ER 4102ST cavity. ESR intensities were extracted from T1–B2 peak-to-peak amplitudes of the ESR signal of enamel. Fitting procedures were carried out with a single saturating exponential function through the pooled ESR experimental data derived from the repeated measurements, with data weighting by the inverse of the squared ESR intensity ($1/I^2$) and following the recommendations in an earlier study[55]. Full details about the experimental conditions and analytical procedure may be found in Supplementary Information 2.

Dose rate evaluation and age calculations. The combined U-series–ESR age of WU1601 was calculated with the DATA programme[56] using the U-series model defined in an earlier study[57]. The following parameters were used for the dose rate evaluation: an alpha efficiency of 0.13 ± 0.02[58], Monte Carlo beta attenuation factors from ref. [59], dose-rate conversion factors from ref. [60], external sediment (beta and gamma) dose rate from the OSL sample PD40, and a depth of 25 ± 10 cm, resulting in an age of 103 +10/−9 ka.

Optically stimulated luminescence dating. Three samples (PD15, PD17 and PD41) were collected from the aeolian sands (Unit 1) underlying the southern marl outcrop (Unit 2, Fig. 1b). A fourth sample (PD40) was taken from the main fossil-bearing bed (Unit 3). Individual quartz grains were measured on a Risø TL/OSL-DA-15 instrument using the single-aliquot regenerative-dose method[61]. The burial dose for each sample (D_b) was calculated using the central age model[62].

Environmental dose rates were determined using a Risø GM-25-5 low-level beta counting system[63] (beta dose rate), field gamma spectrometry (gamma dose rate) and an estimate of the cosmic dose rate derived using site location and present-day sediment burial depths[64]. Full optically stimulated luminescence dating methods and results are presented in Supplementary Section 3. All analyses were carried out in the Royal Holloway Luminescence Laboratory by S.J.A. and R.C.-W.

Age modelling. Chronometric ages for samples from the Al Wusta site were incorporated into a Bayesian sequential phase model implemented in OxCal v4.2[31] (Supplementary Information 4 and Supplementary Fig. 11). The model consists of two discrete phases separated by a hiatus. Phase 1 was defined by the three OSL ages (PD15, 17 and 41) for samples from the aeolian sands (Unit 1) underlying the lacustrine marls (Unit 2). Phase 2 was defined by the ages for the sand (PD40) and fossils (AW-1 and WU1601) from the water-lain sediments (Unit 3) overlying Unit 2. U-series ages for WU1601 and AW-1 were treated as minimum age estimates, whereas PD40 and the combined U-series–ESR age on WU1601 were treated as finite age estimates. Since the Al Wusta sequence accumulated over a short period of time, and contains only five finite ages (and three minimum ages), the general outlier model[31] was unable to function, and instead a simpler model using agreement indices was employed. This analysis yielded A_{model} (76) and $A_{overall}$ (79) values well in excess of the generally accepted threshold (60; ref. [31]), with only one age yielding an individual agreement index below this threshold (PD17, 51). These data indicate that no ages should be excluded from the model, and that the age model itself is robust. The Bayesian sequential model yielded an age for the end of Phase 1 of 93.1 ± 2.6 ka (1σ uncertainties), while Phase 2 yielded start and end dates of 92.2 ± 2.6 ka and 90.4 ± 3.9 ka, respectively. The end date for Phase 2 should be treated as a maximum value since no overlying material is present, precluding the possibility of further constraining the end of this phase.

Stratigraphy and sedimentology. *Sediment analysis.* Bulk samples (in the form of coherent blocks) were taken at 10 cm intervals through each of the marl beds in four sections (Fig. 1c and Supplementary Figs. 13 and 14). Each block was air-dried and subsamples (approximately 0.5 g) were removed, powdered and analysed for percentage carbonate content using Bascomb calcimetry, which measures the volume of carbon dioxide liberated from a known sample mass during reaction with 10% HCl[65]. Thin ections were prepared from fresh sediment blocks. The sediments did not require acetone treatment as they were already dry and, due to their permeability, were impregnated with a bonding resin. Standard thin-section preparation was then carried out using techniques developed in the Centre for Micromorphology at Royal Holloway, University of London[66]. Thin ections were analysed using an Olympus BX-50 microscope with magnifi ations from × 20 to ×200 and photomicrographs were captured with a Pixera Penguin 600es camera. A point-count approach was used to produce semi-quantifi d data from the thin sections, based on counting micro-features at 3 mm intervals along linear transects 1 cm apart. Refs [42,67,68] were referred to when identifying features. X-ray diffraction analysis was carried out at the Department of Earth Sciences (Royal Holloway, University of London). Powdered samples were analysed on a Philips PW1830/3020 spectrometer with copper Kα X-rays. Mineral peaks were identifi d manually from the ICDD Powder Diffraction File database. The methods and results are described further in Supplementary Information 5.

Diatoms. Samples were analysed using a standard method[69] (Supplementary Information 5). Thus, all samples were treated with 30% H_2O_2 and 5% HCl to digest organic material and remove calcium carbonate. Distilled water was added to dilute the samples after heating, which were then stored in the refrigerator for four days to minimize further chemical reactions. The samples were rinsed daily and allowed to settle overnight. A known volume of microspheres was added to the supernatant after the last rinse to enable calculation of the diatom concentration[70]. The slides were air-dried at room temperature in a dust-free environment before mounting with Naphrax diatom mountant. Diatom taxonomy followed previous studies[71–73] and taxonomic revisions[74,75] with at least 300 valves enumerated for a representative sample at ×1,000 magnification.

Prevalent trends in the diatom assemblage were explored using ordination analyses using CANOCO 4.5 of ref. [76]. Detrended correspondence analysis[77] with detrending by segments and down-weighting of rare species was used to investigate taxonomic variations within each site and to determine whether linear or unimodal models should be used for further analyses. If the gradient length of the first axis is < 1.5 s.d. units, linear methods (principle component analysis) should be used; however, if the gradient length is > 1.5 s.d. units, unimodal methods (correspondence analysis) should be used[78]. Detrended canonical correspondence analysis[79]was also used to show changes in compositional turnover scaled in s.d. units. Therefore, variations in the down-core detrended canonical correspondence analysis first-axis sample scores show an estimate of the compositional change between samples along an environmental or temporal gradient. Depth was used as the sole constraint as the samples in each site are in a known temporal order[80]. The data set was square-root-transformed to normalize the distribution before analyses. Optimal sum-of-squares partitioning[81] with the program ZONE[82] and comparison of the zones with the broken-stick model using the program BSTICK[83] were used to determine significant zones. The planktonic/benthic ratio, habitat summary, concentration and the *F* index (a dissolution index[84]) were calculated for all of the samples.

Stable isotopes. It is common practice when analysing the $\delta^{18}O$ and $\delta^{13}C$ values of lacustrine/palustrine carbonates to either: sieve the sediment and analyse the <63 µm fraction; or use the microstructure of the sample, as identified under thin-section analysis, to identify pure, unaltered fabrics, which can then be drilled out and analysed[85]. The former procedure ensures that the analysed fraction comprises pure authigenic marl (rather than a mixture of osctracod, mollusc, chara and marl

components that will contain different isotopic values). The latter is done to ensure that any carbonate that has been affected by diagenesis is sampled. Neither of these approaches were carried out here as: microfabric analysis showed no evidence of diagenesis (although some of the samples are cemented, the cement makes a negligible component of sample mass); and some of the samples have incipient cementation, which means that they cannot be sieved. Bulk carbonate powders were consequently analysed for $\delta^{18}O$ and $\delta^{13}C$. To show that the analysis of bulk samples had no impact on the derived isotopic data, samples that were friable enough to be sieved were treated with sodium hexametaphosphate to disaggregate them and then homogenized and separated into two subsamples for isotopic analysis: a sieved <63 µm fraction and a homogenized bulk sample. The resulting isotopic data showed no difference between the $\delta^{18}O$ and $\delta^{13}C$ values of the sieved and bulk samples (Supplementary Fig. 13b), highlighting that the homogeneous and unaltered nature of the material results in bulk carbonate isotopic analysis generating valid data. Two samples were taken from different locations of each sampled block to generate a larger data set of independent samples. The $\delta^{18}O$ and $\delta^{13}C$ values of each samples were determined by analysing CO_2 liberated from the reaction of the sample with phosphoric acid at 90 °C using a VG PRISM series 2 mass spectrometer in the Earth Sciences Department at Royal Holloway. Internal (RHBNC) and external (NBS19, LSVEC) standards were run every 4 and 18 samples respectively. The 1σ uncertainties are 0.04‰ ($\delta^{18}O$) and 0.02‰ ($\delta^{13}C$). All isotope data presented in this study are quoted against the Vienna PeeDee Belemnite (VPDB) standard.

Vertebrate fossil analyses. Each fossil specimen was identified to the lowest taxonomic and anatomical level possible (Supplementary Fig. 20, Supplementary Table 19 and Supplementary Information 6). Taxonomic identification and skeletal element portions were determined on the basis of anatomical landmarks, and facilitated by comparisons with the Australian National University Archaeology and Natural History reference collection (Canberra), unregistered biological collections held at the University of New South Wales (Sydney) and the large mammal collections of the Zoologische Staatssammlung München (Munich). Each specimen was assigned a size category (small, medium or large) following ref. [86], and corresponding to the five size classes described in ref. [87], where small, medium and large denote size classes 1–2, 3A–3B and 4–6, respectively. Element abundance is reported as the number of identified specimens.

Each specimen was examined for modification by eye and hand-lens (×10) under both natural and high-incidence light, and examined at different angles to assist identification of fine-scale surface modifications. Where required, further examination and photography were carried out using a digital microscope (Model: Dino-lite, AM7013MZ). Morphometric data (length, breadth and width) were measured using digital callipers (Model: Mitutoyo Corp, CD-8"PMX), and specimen weights using a digital scale. Bone surface modifications were identified and recorded following standard methodologies: butchery and tooth marks[88–94], burning[95,96], rodent gnawing[97,98], weathering[99] and trampling[100]. Carnivore damage was categorized as pit, score, furrow or puncture, and the location was noted[94]. Tooth mark morphometric data—short and long axes—was also recorded. Any additional modifications (that is, polish, manganese staining and root etching) were also reported and described. Bone breakage was recorded as green, dry or both, following an earlier study[101]. Long-bone circumference completeness was recorded using the three categories described in ref. [102]: type 1 (<1/2), type 2 (>1/2 but incomplete) and type 3 (complete).

Lithic analysis. Lithics were systematically collected during pedestrian transects and excavations of Al Wusta. This produced a total studied assemblage of 380 lithics (Supplementary Information 7). Further lithics extended for a considerable distance to the north, seeming to track the outlines of the palaeolake, but we conducted detailed analysis only on lithics from the southern part of the site, close to AW-1 and the sedimentary ridge on which it was found (that is, south of the Holocene playa). These were analysed using the methodology described in earlier studies[25,45,103–105]. As well as qualitative analysis of technological features indicating particular techniques and methods of reduction, a variety of quantitative features such as dimensions, the number of scars and percentage of cortex were recorded. Informative examples were selected for photography and illustration. This approach allows both a characterization and description of the assemblage and broad comparison with other assemblages from surrounding regions.

Reporting Summary. Further information on experimental design is available in the Nature Research Reporting Summary linked to this article.

Data availability. All relevant data are included in the paper and/or its Supplementary Information files.

Received: 4 July 2017; Accepted: 26 February 2018;
Published online: 09 April 2018

References

1. Stringer, C. The origin and evolution of *Homo sapiens*. *Phil. Trans. R. Soc. B* **371**, 20150237 (2016).
2. Hershvokitz, I. et al. The earliest modern humans outside Africa. *Science* **359**, 456–459 (2018).
3. Grün, R. et al. U-series and ESR analyses of bones and teeth relating to the human burials from Skhul. *J. Hum. Evol.* **49**, 316–334 (2005).
4. Groucutt, H. S. et al. Rethinking the dispersal of *Homo sapiens* out of Africa. *Evol. Anthropol.* **24**, 149–164 (2015).
5. Petraglia, M. D. et al. Middle Paleolithic assemblages from the Indian subcontinent before and after the Toba super-eruption. *Science* **317**, 114–116 (2007).
6. Bae, C. J. & Douka, K. & Petraglia, M. D. On the origin of modern humans: Asian perspectives. *Science* **358**, eaai9067 (2017).
7. Mellars, P., Gori, K. C., Carr, M., Soares, P. A. & Richards, M. B. Genetic and archaeological perspectives on the initial modern human colonization of southern Asia. *Proc. Natl Acad. Sci. USA* **110**, 10699–10704 (2013).
8. Shea, J. J. Transitions or turnovers? Climatically-forced extinctions of *Homo sapiens* and Neanderthals in the east Mediterranean Levant. *Quatern. Sci. Rev.* **27**, 2253–2270 (2008).
9. Mallick, S. et al. The Simons Genome Diversity Project: 300 genomes from 142 diverse populations. *Nature* **538**, 201–206 (2016).
10. Pagani, L. et al. Genomic analyses inform on migration events during the peopling of Eurasia. *Nature* **538**, 238–242 (2016).
11. Groucutt, H. S. et al. Stone tool assemblages and models for the dispersal of *Homo sapiens* out of Africa. *Quatern. Int.* **382**, 8–30 (2015).
12. Demeter, F. et al. Early modern humans from Tam Pà Ling, Laos: fossil review and perspectives. *Curr. Anthropol.* **57**, S17 (2017).
13. Westaway, K. E. et al. An early modern human presence in Sumatra 73,000–63,000 years ago. *Nature* **548**, 322–325 (2017).
14. Michel, V. et al. The earliest modern *Homo sapiens* in China? *J. Hum. Evol.* **101**, 101–104 (2016).
15. Liu, W. et al. The early unequivocally modern humans in southern China? *Nature* **526**, 696–699 (2015).
16. Bae, C. et al. Modern human teeth from Late Pleistocene Luna Cave (Guangxi, China). *Quatern. Int.* **354**, 169–183 (2015).
17. Liu, W. et al. Human remains from Zhiredong, South China, and modern human emergence in East Asia. *Proc. Natl Acad. Sci. USA* **107**, 19201–19206 (2010).
18. Clarkson, C. et al. Human occupation of northern Australia by 65,000 years ago. *Nature* **547**, 306–310 (2017).
19. Martinón-Torres, M., Wu, X., de Castro, J. M. B., Xing, S. & Liu, W. *Homo sapiens* in the eastern Asian Late Pleistocene. *Curr. Anthropol.* **58**, S17 (2017).
20. Groucutt, H. S. & Petraglia, M. D. The prehistory of Arabia: deserts, dispersals and demography. *Evol. Anthropol.* **21**, 113–125 (2012).
21. Petraglia, M. D., Groucutt, H. S., Parton, A. & Alsharekh, A. Green Arabia: human prehistory at the cross-roads of continents. *Quatern. Int.* **382**, 1–7 (2015).
22. Jennings, R. P. et al. The greening of Arabia: multiple opportunities for human occupation in the Arabian Peninsula during the Late Pleistocene inferred from an ensemble of climate model simulations. *Quatern. Int.* **205**, 181–199 (2015).
23. Rosenberg, T. M. et al. Middle and Late Pleistocene humid periods recorded in palaeolake deposits in the Nafud desert, Saudi Arabia. *Quatern. Sci. Rev.* **70**, 109–123 (2013).
24. Breeze, P. S. et al. Palaeohydrological corridors for hominin dispersals in the Middle East ~250–70,000 years ago. *Quatern. Sci. Rev.* **11**, 155–185 (2016).
25. Scerri, E. M. L., Drake, N. A., Jennings, R. & Groucutt, H. S. Earliest evidence for the structure of *Homo sapiens* populations in Africa. *Quatern. Sci. Rev.* **101**, 207–216 (2014).
26. Trinkaus, E. *The Shanidar Neandertals* (Academic, New York, 1981).
27. McCown, T. D. & Keith, A. *The Stone Age of Mount Carmel* Vol. 2 (Clarendon Press, Oxford, 1939).
28. Vandermeersch, B. *Les Hommes Fossiles de Qafzeh (Israel)* (CNRS, Paris, 1981).
29. Walker, M. J., Ortega, J., López, M. V., Parmová, K. & Trinkaus, E. Neanderthal postcranial remains from the Sima de las Palomas del Cabezo Gordo, Murcia, southeastern Spain. *Am. J. Phys. Anthropol.* **144**, 505–515 (2011).
30. Benjamin, M. et al. Where tendons and ligaments meet bone: attachment sites ('entheses') in relation to exercise and/or mechanical load. *J. Anat.* **208**, 471–490 (2006).
31. Bronk Ramsey, C. Bayesian analysis of radiocarbon dates. *Radiocarbon* **51**, 337–360 (2009).
32. Drake, N. A., Breeze, P. & Parker, A. Palaeoclimate in the Saharan and Arabian deserts during the Middle Palaeolithic and the potential for hominin dispersals. *Quatern. Int.* **300**, 48–61 (2013).
33. Parton, A. et al. Orbital-scale climate variability in Arabia as a potential motor for human dispersals. *Quatern. Int.* **382**, 82–97 (2015).
34. Vaks, A., Bar-Matthews, M., Matthews, A., Ayalon, A. & Frumkin, A. Middle–Late Quaternary paleoclimate of northern margins of the

Saharan–Arabian desert: reconstruction from speleothems of Negev desert, Israel. *Quatern. Sci. Rev.* **29**, 2647–2662 (2010).
35. Grant, K. M. et al. The timing of Mediterranean sapropel deposition relative to insolation, sea-level and African monsoon changes. *Quatern. Sci. Rev.* **140**, 125–141 (2016).
36. Bar-Matthews, M., Ayalon, A., Gilmour, M., Matthews, A. & Hawkesworth, C. J. Sea-land oxygen isotopic relationships from planktonic foraminifera and speleothems in the eastern Mediterranean region and their implication for paleorainfall during interglacial intervals. *Geochim. Cosmochim. Acta* **67**, 3181–3199 (2003).
37. Lisiecki, L. E. & Raymo, M. E. A Pliocene–Pleistocene stack of 57 globally distributed benthic $\delta^{18}O$ records. *Paleoceanography* **20**, 1–17 (2005).
38. Berger, A. & Loutre, M. F. Insolation values for the climate of the last 10 million years. *Quatern. Sci. Rev.* **10**, 297–317 (1991).
39. Fleitmann, D., Burns, S. J., Neff, U., Mangini, A. & Matter, A. Changing moisture sources over the last 333,000 years in northern Oman from fluid-inclusion evidence in speleothems. *Quatern. Res.* **60**, 223–232 (2003).
40. Rosenberg, T. M. Humid periods in southern Arabia: windows of opportunity for modern human dispersal. *Geology* **39**, 1115–1118 (2011).
41. Clark-Balzan, L., Parton., A., Breeze, P. S., Groucutt, H. S. & Petraglia, M. D. Resolving problematic luminescence chronologies for carbonate- and evaporite-rich sediments spanning multiple humid periods in the Jubbah Basin, Saudi Arabia. *Quatern. Geochron.* **50**, 50–73 (2018).
42. Alonso-Zarza, A. M. Palaeoenvironmental signifi ant of palustrine carbonates and calcretes in the geological record. *Earth Sci. Rev.* **60**, 261–298 (2003).
43. Estes, R. D. *The Behaviour Guide to African Mammals*. (Univ. California Press, Berkeley, 1991).
44. O'Regan, H. J., Turner, A., Bishop, L. C., Elton, S. & Lamb, A. L. Hominins without fellow travellers? First appearances and inferred dispersals of Afro-Eurasian large-mammals in the Plio-Pleistocene. *Quatern. Sci. Rev.* **30**, 1343–1352 (2011).
45. Groucutt, H. S. et al. Human occupation of the Arabian Empty Quarter during MIS 5: evidence from Mundafan al-Buhayrah. *Quatern. Sci. Rev.* **119**, 116–135 (2015).
46. Millard, A. R. A critique of the chronometric evidence for hominid fossils: I. Africa and the Near East 500–50 ka. *J. Hum. Evol.* **54**, 848–874 (2008).
47. Hublin, J. J. et al. New fossils from Jebel Irhoud, Morocco and the pan-African origin of *Homo sapiens*. *Nature* **546**, 289–292 (2017).
48. Richter, D. et al. The age of the hominin fossils from Jebel Irhoud, Morocco, and the origins of the Middle Stone Age. *Nature* **546**, 293–296 (2017).
49. Stimpson, C. et al. Middle Pleistocene vertebrate fossils from the Nefud desert, Saudi Arabia: implications for biogeography and palaeoecology. *Quatern. Sci. Rev.* **143**, 13–36 (2016).
50. O'Higgins, P. & Jones, N. Facial growth in *Cercocebus torquatus*: an application of three-dimensional geometric morphometric techniques to the study of morphological variation. *J. Anat.* **193**, 251–272 (1998).
51. R Core Team *R: A Language and Environment for Statistical Computing* (R Foundation for Statistical Computing, Vienna, 2015); http://www.R-project.org
52. Klingenberg, C. P. MorphoJ: an integrated software package for geometric morphometrics. *Mol. Ecol. Resour.* **11**, 353–357 (2011).
53. Grün, R., Eggins, S., Kinsley, L., Mosely, H. & Sambridge, M. Laser ablation U-series analysis of fossil bones and teeth. *Palaeogeogr. Palaeoclimatol. Palaeoecol.* **416**, 150–167 (2014).
54. Benson, A. et al. Laser ablation depth profiling of U-series and Sr isotopes in human fossils. *J. Arch. Sci.* **40**, 2991–3000 (2013).
55. Duval, M. & Grün, R. Are published ESR dose assessments on fossil tooth enamel reliable? *Quat. Geochron.* **31**, 19–27 (2016).
56. Grün, R. The DATA program for the calculation of ESR age estimates on tooth enamel. *Quatern. Geochron.* **4**, 231–232 (2009).
57. Grün, R., Schwarcz, H. P. & Chadam, J. ESR dating of tooth enamel: coupled correction for U-uptake and U-series disequilibrium. *Int. J. Radiat. Appl. Instrum. D* **14**, 237–241 (1988).
58. Grün, R. & Katzenberger-Apel, O. An alpha irradiator for ESR dating. *Anc. TL* **12**, 35–38 (1994).
59. Marsh, R. E *Beta-Gradient Isochrons Using Electron Paramagnetic Resonance: Towards a New Dating Method in Archaeology*. MSc thesis, McMaster Univ. (1999).
60. Guérin, G., Mercier, N. & Adamiec, G. Dose-rate conversion factors: update. *Anc. TL* **29**, 5–8 (2011).
61. Murray, A. S. & Wintle, A. G. Luminescence dating of quartz using an improved single-aliquot regenerative-dose protocol. *Radiat. Meas.* **32**, 57–73 (2000).
62. Galbraith, R. F., Roberts, R. G., Laslett, G. M., Yoshida, H. & Olley, J. M. Optical dating of single and multiple grains of quartz from Jinmium rock shelter, northern Australia: Part I, experimental design and statistical models. *Archaeometry* **41**, 339–364 (1999).
63. Bøtter-Jensen, L. & Mejdahl, V. Assessment of beta dose-rate using a GM multicounter system. *Int. J. Rad. Appl. Instrum. B* **14**, 187–191 (1988).
64. Prescott, J. R. & Hutton, J. T. Cosmic ray and gamma ray dosimetry for TL and ESR. *Int. J. Rad. Appl. Instrum. D* **14**, 223–227 (1988).
65. Gale, S. & Hoare, P. *Quaternary Sediments: Petrographic Methods for the Study of Unlithified Rocks* (Belhaven and Halsted Press, London, 1991).
66. Palmer, A. P., Lee, J. A., Kemp, R. A. & Carr, S. J. *Revised Laboratory Procedures for the Preparation of Thin Sections from Unconsolidated Sediments* (Centre for Micromorphology Publication, Royal Holloway, Univ. London, 2008).
67. Kemp, R. A. *Soil Micromorphology and the Quaternary* (Quaternary Research Association, 1985).
68. Stoops, G. *Interpretation of Micromorphological Features of Soils and Regoliths* (Elsevier, Amsterdam, 2010).
69. Rengberg, I. A procedure for preparing large sets of diatom sets from sediment. *J. Palaeolimnol.* **4**, 87–90 (1990).
70. Battarbee, R. W. & Knen, M. J. The use of electronically counter microspheres in absolute diatom analysis. *Limnol. Oceanogr.* **27**, 184–188 (1982).
71. Krammer, K. & Lange-Bertalot, H. *Bacillariophyceae 2. Teil Epithemiaceae, Suirellaceae* (Gustav-Fischer Verlag, Stuttgart, 1988).
72. Krammer, K. & Lange-Bertalot, H. *Bacillariophyceae 3. Teil Centrales, Fragicariaceaa, Eunotiacea* (Gustav-Fischer Verlag, Stuttgart, 1991).
73. Krammer, K. & Lange-Bertalot, H. *Bacillariophyceae 4. Teil Achnanthaceae, Kritshe Ergänzungen zu Navicula (Lineolate) und Gomphonema* (Gustav-Fischer Verlag, Stuttgart, 1991).
74. Crawford, R. M., Likhoshway, Y. V. & Jahn, R. Morphology and identity of *Aulacoesiera italic* and typifi ation of *Aulacoseira* (Bacillariophyta). *Diatom Res.* **18**, 1–19 (2003).
75. Navok, T., Guillory, W. X., Julius, M. L., Theriort, E. C. & Alverson, A. J. Towards a phylogenetic classifi ation of species belonging to the diatom genus *Cyclotella* (Bacillariophyceae): transfer of species formerly placed in *Puncticulata, Handmannia, Pliocaenicus* and *Cyclotella* to the genus *Lindavia*. *Phytotaxa* **217**, 249–264 (2015).
76. Ter Braak, C. J. F. & Šmilauer, P. *CANOCO Reference Manual and CanoDraw for Windows User's Guide: Soft are for Canonical Community Ordination* Version 4.5 (Microcomputer Power, 2002).
77. Hill, M. O. & Gauch, H. G. Detrended correspondence analysis: an improved ordination technique. *Plant Ecol.* **42**, 47–58 (1980).
78. Ter Braak, C. J. F. & Prentice, I. C. A theory of gradient analysis. *Adv. Ecol. Res.* **18**, 271–317 (1988).
79. Ter Braak, C. J. F. Canonical correspondence analysis: a new eigenvector technique for multivariate direct gradient analysis. *Ecology* **67**, 1167–1179 (1986).
80. Smol, J. P. et al. Climate-driven regime shifts in the biological communities of arctic lakes. *Proc. Natl Acad. Sci. USA* **102**, 4397–4402 (2005).
81. Birks, H. J. B. & Gordon, A. D. *Numerical Methods in Quaternary Pollen Analysis* (Academic, London, 1985).
82. Juggins, S. *ZONE Soft are* Version 1.2. (Univ. Newcastle, 1985).
83. Bennett, K. D. Determination of the number of zones in a biostratigraphical sequence. *New Phytol.* **132**, 155–170 (1996).
84. Ryves, D. B., Juggins, S., Fritz, S. C. & Battarbee, R. W. Experimental diatom dissolution and the quantifi ation of microfossil preservation in sediments. *Palaeogeogr. Palaeoclimatol. Palaeoecol.* **172**, 99–113 (2001).
85. Candy, I. et al. The evolution of Palaeolake Flixton and the environmental context of Starr Carr: an oxygen and carbon isotopic record of environmental change for the early Holocene. *Proc. Geol. Assoc.* **126**, 60–71 (2015).
86. Domínguez-Rodrigo, M., Barba, R., De la Torre, I. & Mora, R. in *Deconstructing Olduvai: A Taphonomic Study of the Bed I Sites* (eds Domínguez-Rodrigo, M. et al.) 101–125 (Springer, New York, 2007).
87. Bunn, H. T. *Meat-Eating and Human Evolution: Studies on the Diet and Subsistence Patterns of Plio-Pleistocene Hominids in East Africa.* PhD thesis, Univ. Wisconsin (1982).
88. Bunn, H. T. & Kroll, E. M. Systematic butchery by Pilo/Pleistocene hominids at Olduvai Gorge, Tanzania. *Curr. Anthropol.* **27**, 431–452 (1986).
89. Binford, L. R. *Faunal Remains from Klasies River Mouth* (Academic, New York, 1984).
90. Andrews, P. & Cook, J. Natural modifi ations to bones in a temperature setting. *Man* **20**, 675–691 (1985).
91. Blumenschine, R. J. & Selvaggio, M. M. Percussion marks on bone surfaces as a new diagnostic of hominid behaviour. *Nature* **333**, 763–765 (1988).
92. Fisher, J. W. Bone surface modifi ations in zooarchaeology. *J. Archaeol. Method Th ory* **2**, 7–68 (1995).
93. Noe-Nygaard, N. Man-made trace fossils on bones. *J. Hum. Evol.* **4**, 461–461 (1989).
94. Binford, L. R. *Bones: Ancient Men and Modern Myths* (Academic, New York, 1981).

95. Stiner, M., Kuhn, S., Weiner, S. & Bar-Yosef, O. Differential burning, recrystallization, and fragmentation of archaeological bone. *J. Archaeol. Sci.* **22**, 223–237 (1995).
96. Shipman, P., Foster, G. & Schoeninger, M. Bunt bones and teeth: an experimental study of color, morphology, crystal structure and shrinkage. *J. Archaeol. Sci.* **11**, 307–325 (1984).
97. Tong, H. W., Zhang, S., Chen, F. & Li, Q. Rongements sélectifs des os par les porcs-épics et autres rongeurs: cas de la grotte Tianyuan, un site avec des restes humains fossiles récemment découvert près de Zhoukoudian (Choukoutien). *Anthropologie* **112**, 353–369 (2008).
98. Dart, R. A. Bone tools and porcupine gnawing. *Am. Anthropol.* **60**, 715–724 (1958).
99. Behrensmeyer, A. K. Taphonomic and ecological information from bone weathering. *Paleobiology* **4**, 150–162 (1978).
100. Behrensmeyer, A. K., Gordon, K. & Yanagi, G. T. Trampling as a cause of bone surface damage and psuedo-cutmarks. *Nature* **319**, 402–403 (1986).
101. Villa, P. & Mahieu, E. Breakage pattern of human long bones. *J. Hum. Evol.* **21**, 27–48 (1991).
102. Bunn, H. T. in *Animals and Archaeology* Vol. 1 (eds Clutton-Brock, J. & Grigson, C.) 143–148 (BAR International Series 163, Oxford, 1983).
103. Scerri, E. M. L., Groucutt, H. S., Jennings, R. P. & Petraglia, M. D. Unexpected technological heterogeneity in northern Arabia indicates complex Late Pleistocene demography at the gateway to Asia. *J. Hum. Evol.* **75**, 125–142 (2014).
104. Scerri, E. M. L., Gravina, B., Blinkhorn, J. & Delagnes, A. Can lithic attribute analyses identify discrete reduction trajectories? A quantitative study using refitted lithic sets. *J. Arch. Method Theory* **23**, 669–691 (2016).
105. Groucutt, H. S. et al. Late Pleistocene lakeshore settlement in northern Arabia: Middle Palaeolithic technology from Jebel Katefeh, Jubbah. *Quatern. Int.* **382**, 215–236 (2016).

Acknowledgements

We thank HRH Prince Sultan bin Salman bin Abdulaziz Al-Saud, President of the Saudi Commission for Tourism and National Heritage (SCTH), and A. Ghabban, Vice President of the SCTH for permission to carry out this study. Z. Nawab, President of the Saudi Geological Survey, provided research support and logistics. Fieldwork and analyses were funded by the European Research Council (no. 295719, to M.D.P. and 617627, to J.T.S.), the SCTH, the British Academy (H.S.G. and E.M.L.S.), The Leverhulme Trust, the Australian Research Council (DP110101415 to R.G., ARC Future Fellowship Grant FT150100215 to M.D., and FT160100450 to J.L.), European Union Marie Curie International Outgoing Fellowship (PIOF-GA-2013-626474, to M.D.), and the Research Council of Norway (SFF Centre for Early Sapiens Behaviour, 262618). We thank P. Cuthbertson, K. Janulis, M. Bernal, S. Al-Soubhi, M. Haptari, A. Matari and Y. Al-Mufarreh for assistance in the field. We thank I. Cartwright (Institute of Archaeology, University of Oxford) for the photographs of AW-1 (Fig. 2a), I. Matthews (RHUL) for producing the Bayesian age model and M. O'Reilly (MPI-SHH) for assistance with the preparation of figures. We acknowledge the Max Planck Society for supporting us with comparative fossil data, and we thank curators for access to comparative extant and fossil material in their care (Supplementary Tables 5 and 7). Maps were created using ArcGIS software by Esri.

Author contributions

H.S.G. and M.D.P. designed, coordinated and supervised the study. H.S.G., I.S.A.Z., N.A.D., S.J.A., I.C., R.C.-W., J.L., P.S.B., M.S., G.J.P., A.A., A.A.-O., M.Z., A.M.M, K.S.M.A, B.Z, E.M.L.S and M.D.P conducted excavation, survey and multidisciplinary sampling at Al Wusta. L.T.B., T.L.K., E.P., N.B.S. and J.T.S. conducted the morphological analysis and comparative study of the AW-1 phalanx. R.G., M.D. and L.K. carried out the U-series and ESR analyses. S.J.A. and R.C.-W carried out the OSL dating. I.C. and R.C.-W conducted the stratigraphic and sedimentological analysis of the site, with input from N.A.D., J.L. and G.J.P. W.W.S. analysed the diatoms. M.S. and J.L. analysed the vertebrate fossils, with input from G.J.P. Lithic analysis was conducted by H.S.G. and E.M.L.S. Spatial analyses were conducted by P.S.B. All authors helped to write the paper.

Competing interests

The authors declare no competing interests.

Additional information

Supplementary information is available for this paper at https://doi.org/10.1038/s41559-018-0518-2.

Reprints and permissions information is available at www.nature.com/reprints.

Correspondence and requests for materials should be addressed to H.S.G. or M.D.P.

Publisher's note: Springer Nature remains neutral with regard to jurisdictional claims in published maps and institutional affiliations.